# *Trans*−*Cis* Isomerization of Proline 22 in Bovine Prothrombin Fragment 1: A Surprising Result of Structural Characterization†

Lalith Perera,‡ Thomas A. Darden,§ and Lee G. Pedersen*,‡,§

*Department of Chemistry, University of North Carolina, Chapel Hill, North Carolina 27599-3290, and National Institute of Environmental Health Sciences, Research Triangle Park, North Carolina 27709*

*Received February 2, 1998; Revised Manuscript Received April 29, 1998*

ABSTRACT: The calcium ion-mediated interaction of bovine prothrombin (BF1) with negatively charged phospholipid membranes is assumed to be largely via the Gla domain of BF1 with the fold of the Gla domain essential for binding. It has been reported that Pro22 undergoes classical *trans* to *cis* isomerization in the presence of calcium ions with the *cis* conformation of Pro22 of BF1 responsible for membrane binding [Evans, T. C., Jr., and Nelsestuen, G. L. (1996) *Biochemistry 35*, 8210−8215]. However, Pro22 was found to be in the *trans* conformation in the crystal structure of BF1. In the present work, we have used molecular dynamics simulations to investigate the relative importance of the two conformations of Pro22 to the structural and dynamical properties of BF1. The initial *trans* conformation of Pro22 in BF1 was slowly converted to *cis*-Pro22 using constrained dynamics. The second-generation AMBER force field in conjunction with the particle mesh Ewald method to accommodate long-range interaction was employed in the trajectory calculations. Comparison of the BF1(*trans*-Pro22) and BF1(*cis*-Pro22) equilibrated structures reveals *surprisingly* that the overall structural changes associated with the *trans*−*cis* isomerization is minimal and only minor modifications to the hydrogen bond network and the network of N-terminus Ala1 take place. The calculated electrostatic potential energy surfaces of the two protein structures also appear to be very similar, indicating the near equality of the local interaction site environments in the protein prior to lipid binding.

In small peptide synthesis, the peptide bond at the amino terminus of the proline is found to be in the *trans* conformation, but in detailed protein structures, about 15% of these bonds are determined to be in the *cis* conformation (*18*). The small difference in free energy between *cis* and *trans* conformers leads to a variable relative population of states that may have relevance in the protein folding process (*11*, *19*, *33*).

Prothrombin, a central protein in the coagulation cascade, is converted to thrombin on the membrane surface by the macromolecular complex of factor Xa and factor Va. Presence of calcium ions promotes the formation of correct protein conformation and is also essential and specific for membrane binding (*32*). Upon addition of metal ions, Nelsestuen (*28*) showed a biphasic fluorescence quenching behavior for BF1[1] [initial rapid phase (<1 s) followed by a slow quenching (>10 min)]. Marsh et al. (*24*) hypothesized that the slow quenching was due to the *trans*−*cis* isomerization of Pro22. Subsequent fluorescence quenching experiments suggested that, in the process of phospholipid binding, Pro22 of BF1 may undergo isomerization from the *trans* to *cis* conformation in a step essential for membrane binding (*10*). The 1−45 residue peptide of BF1, which Pollock et al. (*32*) earlier demonstrated retains BF1 binding properties, was employed in the fluorescent quenching experiments. In the X-ray crystal structure of BF1, however, Pro22 was found in the *trans* conformation (*35*).

The usefulness of molecular dynamics simulation techniques for the study of the *cis*/*trans* isomerization of proline in staphylococcal nuclease has recently been demonstrated (*16*, *17*). These rather limited simulations correctly predict small differences in the free energies between the *cis* and *trans* forms composed of larger, compensating differences in enthalpy and entropy. In their MD simulation study, Charifson et al. (*3*) observed an unforced transition from the *trans* to *cis* conformer for Pro22 during a 107 ps trajectory calculation of the BF1(residues 1−65)−calcium complex. This MD simulation was state of the art in 1991, but substantial progress has been made in dealing with long-range forces since then (see below). The starting *trans* conformation, which was modeled from a lower resolution (2.8 Å) X-ray crystal structure (*36*), was retained for the first 80 ps and then underwent isomerization to the *cis* conformer. They estimated the *cis* conformation to be energetically favored by about 17 kcal/mol with an activation barrier of ∼9 kcal/mol (*trans* → *cis*). $^{13}C$ and $^{1}H$ NMR studies in aqueous solutions showed that $\Delta G$ of the isomerization of proline in small cyclic peptides to be on the order of 15 kcal/

† This work was supported by National Institutes of Health Grant HL-06350 (to L.G.P.).

* Author to whom correspondence should be addressed at the University of North Carolina: telephone (919) 962-1578; fax (919) 962-2388; e-mail pedersen@niehs.nih.gov.

‡ University of North Carolina, Chapel Hill.

§ National Institute of Environmental Health Sciences.

[1] Abbreviations: Gla, γ-carboxyglutamic acid; BF1, bovine prothrombin fragment 1; Gla domain, residues 1−45 in bovine prothrombin fragment 1; BF1(*trans*-Pro22), bovine prothrombin fragment 1 with *trans*-Pro22; BF1(*cis*-Pro22), bovine prothrombin fragment 1 with *cis*-Pro22; VKD, vitamin K dependent; RMSD, root-mean-square deviation.

S0006-2960(98)00263-3 CCC: $15.00 
Published on Web 07/17/1998

mol (*7*). Charifson et al. (*3*) suggested that the activation energy for the isomerization reaction was provided by release of intramolecular crystal packing forces in the solution simulation. However, Hamaguchi et al. (*15*) did not observe this isomerization process from the 116 ps molecular dynamics simulation of BF1 in solution (N-terminal residues from 1 to 145 with Pro22 in the *trans* conformation) using an improved force field which partially, but not completely, accommodated long-range interactions.

Here, we reexamine the *trans*−*cis* isomerization of Pro22 in BF1 (residues 1−45). We have used molecular dynamics simulation techniques to generate equilibrated solution conformations of BF1 in both *cis* and *trans* forms. The second-generation AMBER force field (*6*) in conjunction with the particle mesh Ewald method (*9*) to accommodate, essentially completely, the long-range electrostatic interactions was utilized. Previous MD simulations (*3, 15*) lacked explicit methods for accounting completely for the long-range electrostatic interactions. Thus, it is important to reevaluate the time-dependent structure of BF1 (residues 1−45) using the higher resolution (2.2 Å) X-ray crystal structure (*35*) and using the substantially improved MD methodology. The solution structures of BF1 with *cis* and *trans* are compared, and the sites thought to be responsible for phospholipid binding are closely examined.

## COMPUTATIONAL PROCEDURE

*Model Construction and Simulation Protocol*. The initial structure of the model protein (BF1 residues 1−45) was derived from the crystallographic coordinates of the BF1/Ca fragment (*35*) for which Pro22 is in the *trans* conformation. The sequence of this fragment is ANKGFLXXVR KGNLXRXCLX XPCSRXXAFX ALXSLSLTDA FWAKY, in which X represents Gla. Necessary hydrogen atoms were added to the X-ray crystallographic structure followed by an energy minimization using a distance-dependent dielectric function. The original BF1 crystallographic water molecules were preserved along with the positions of calcium ions. The protein was then solvated in a box of water molecules so that the box boundaries are at least 12.5 Å away from any protein atom, and any water molecule with its oxygen or hydrogen atoms found within 2.0 Å to any atom in the protein was removed. In the first step, only the added water molecules were energy minimized, and then all the water molecules were used in the minimization, and finally, the whole system was energy minimized. The system was then subjected to a slow heat-up procedure to bring the temperature of the system up to 300 K. After 50 ps of a constant volume−constant temperature simulation, an unrestrained constant pressure−constant temperature protocol was adopted to simulate 800 ps of unrestrained dynamics at the *trans* conformation.

The conversion of *trans*- to *cis*-Pro22 was achieved through the following procedure. The dihedral angle, Cα−C−N−Cα, in which N and the following Cα belong to Pro22, was incrementally decreased from its *trans* value (theoretically 180°) to a value nearer the *cis* conformation (around 0°). The initial structure for this procedure was selected to be that of 200th ps of the above described MD trajectory. The decrement was 2° at a time, and by holding this dihedral angle fixed, the system was subjected to 5 ps of constant volume−constant temperature molecular dynamics. The dihedral angle of the final configuration was reduced by 2°, and this procedure was continued until the *trans*−*cis* isomerization was complete (using 84 segments of 5 ps trajectories, totaling 420 ps of molecular dynamics at constant volume−constant temperature). The final configuration was further subjected to a 50 ps constant volume−constant temperature simulation, followed by a 400 ps constant pressure−constant temperature simulation at the *cis* conformation (unrestrained). During the initial and final molecular dynamic trajectory calculations, no attempt was made to constrain the *trans* or *cis* conformations, respectively.

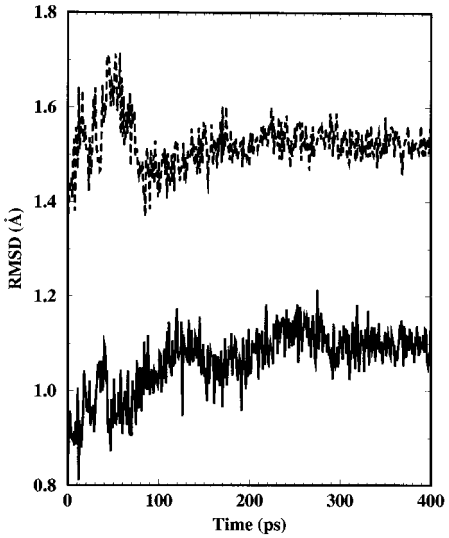


FIGURE 1: Root-mean-square deviations of the backbone atoms calculated with respect to the crystal coordinates: BF1 with *trans*-Pro22 (solid line); BF1 with *cis*-Pro22 (dotted line). Results for the *trans* conformation are shown from the interval between 400 and 800 ps.

In the present study, we used the second-generation AMBER force field (*6*) in conjunction with the particle mesh Ewald method (*9*) to accommodate long-range interactions in all the trajectory calculations associated with solution simulations. The system contained 6083 water molecules and 7 calcium ions. The unit cell was electrically neutral with a total number of 18 983 atoms. All energy minimizations were performed using 100 conjugate gradient steps followed by 10000 steepest descent steps. AMBER version 4.1 (*30*) was used in the trajectory calculations. The time step was 1 fs, and the nonbonded interactions were updated at every fifth step in all simulations.

## RESULTS AND DISCUSSION

*Global Aspects of the Simulations*. We begin the discussion with an assessment of how well the molecular dynamics simulations capture the equilibrium properties of both BF1(*trans*-Pro22) and BF1(*cis*-Pro22) systems. We have used the results of the dynamics of the final 400 ps in this analysis. In Figure 1, we display the RMSDs of the backbone atoms of both BF1(*trans*-Pro22) and BF1(*cis*-Pro22) with respect to the crystal configuration. The leveling off of the values of RMSDs with smaller fluctuations during the last 100 ps shows that both systems have stabilized at equilibration. The stability of the energies of both systems and their components provides supporting evidence for the stability of the system. In addition, the densities fluctuate

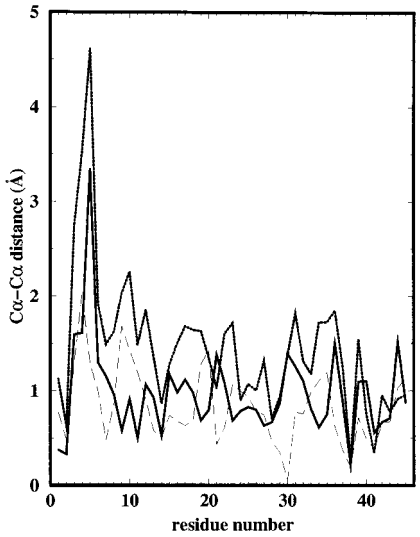


FIGURE 2: Cα−Cα distances. The distances were measured after the optimal backbone alignments of the first 36 residues. Solid line: BF1 with *trans*-Pro22 vs the crystal. Dotted line: BF1 with *cis*-Pro22 vs the crystal. Dashed line: BF1 with *trans*-Pro22 vs BF1 with *cis*-Pro22.

about 1.06 g/cm$^3$ during the last 100 ps of the trajectories. This small fluctuation in density (or the volume of the central box, since the number of particles remains constant) during the final 100 ps of the trajectory calculation is a consequence of the relative consistency in the box dimensions. Since the desired pressure is maintained by the rescaling of the box, dimension consistency serves as a good indicator that the system is in a relaxed configuration.

Smaller magnitudes of RMSDs indicate that the backbone structure (or the secondary structure) of BF1(*trans*-Pro22) in solution closely follows that of the crystal structure (simulated final average RMSD is around 1 Å). However, the difference between the final average RMSD values of the two forms is only about 0.6 Å, and a discernible global change in the secondary structure between the two forms is not apparent.

To more closely study possible differences in the secondary structures, we have compared the deviations of Cα positions with respect to the crystal structure after optimal alignment (see Figure 2). For this purpose, we have selected the final configurations of the two MD trajectories [with BF1(*trans*-Pro22) and BF1(*cis*-Pro22)]. These appear to be reasonably representative configurations since they did not undergo significant structural changes during the last 25 ps. The largest deviation of the Cα positions is consistently found at Phe5 for both systems when compared with the crystal structure. In the crystal structure, Phe5 has the largest *B*-factors, indicating higher uncertainty of the assignments of the coordinates of this residue. In general, BF1(*cis*-Pro22) appears to have somewhat larger deviations when compared with the crystal structure, but the statistical significance of this difference is questionable. The deviations of *trans* versus *cis* (which are included in Figure 2) are relatively small (note that all the values are under 2 Å), and even the disulfide loop region (residues 18−23), which is expected to show larger deviations due to *trans*−*cis* isomerization of Pro22 present in this region, does not display any significant change in the deviation when compared to other deviations.

Table 1: Comparison of the Ala1−N Network for the Solution Structures of *trans*-BF1 and *cis*-BF1[a]

| | donor | acceptor | distance (Å) | angle (deg) |
|---|---|---|---|---|
| *trans*-Pro22 | Ala1−N | Gla17−OE3 | 2.9 | 141 |
| | Ala1−N | Gla21−OE4 | 2.9 | 124 |
| | Ala1−N | Pro22−O | 2.9 | 136 |
| | Ala1−N | Gla27−OE3 | 3.0 | 146 |
| | Ala1−N | Gla27−OE4 | 3.0 | 132 |
| | Ala1−N | Ca−4 | 4.35 | |
| | Ala1−N | Ca−5 | 4.36 | |
| *cis*-Pro22 | Ala1−N | Gla17−OE3 | 2.9 | 136 |
| | Ala1−N | Gla21−OE4 | 2.9 | 133 |
| | Ala1−N | Gla27−OE3 | 2.8 | 136 |
| | Ala1−N | Gla27−OE4 | 2.7 | 117 |
| | Ala1−N | Ca−4 | 4.11 | |
| | Ala1−N | Ca−5 | 4.10 | |
| crystal | Ala1−N | Gla17−OE3 | 2.5 | |
| | Ala1−N | Gla21−OE4 | 2.9 | |
| | Ala1−N | Pro22−O | 3.6 | |
| | Ala1−N | Gla27−OE3 | 4.2 | |
| | Ala1−N | Gla27−OE4 | 3.0 | |
| | Ala1−N | Ca−4 | 2.48 | |
| | Ala1−N | Ca−5 | 3.77 | |

[a] The distances and angles were averaged over the last 20 ps of the MD trajectories. The corresponding distances of the donor and acceptor atoms in the crystal configuration are also included for comparison. The cutoff distance and angle were 3.1 Å and 115°, respectively, for the hydrogen bonds.

The crystallographic *B*-factors calculated from the dynamical trajectories of the solution structure and those evaluated from experiments are closely comparable in magnitudes. The *B*-factors of BF1 averaged over residues 1−45 were 25.2, 23.5, and 19.0 Å$^2$ for the crystal, solution with *trans*-Pro22, and the solution with *cis*-Pro22, respectively. On the average, the magnitudes in the *B*-factor in the solution structure correspond to approximately an angstrom of relative fluctuations of the atoms around their average positions.

*Gla Domain Structure*. In the evaluation of the structural changes associated with the *trans*−*cis* isomerization, we report the results obtained from the last 20 ps of each trajectory and compare them with each other and also with the crystal structure. In addition to the N-terminal Ala1 network, the Gla−calcium network, and the network formed by the calcium ions observed in previous experimental and simulation work, we also compare the hydrogen bonding associated with the disulfide loop region.

*(A) Ala1 Network*. The hydrogen bonding interactions of Ala1 to the inside of the Gla domain are believed to maintain the appropriate shape of the Ω-loop (residues 1−11) for prothrombin binding to membrane surfaces (*40*). In crystallographic BF1, Ala1−N is bound by several hydrogen bonds to Gla17, to the conserved disulfide loop (residues between Cys18 and Cys23), and to the Gla residues immediately following this loop. Two calcium ions are also involved in the formation of this network (Table 1). Both simulation systems (*cis* and *trans*) are found to be consistent with the above description and the exception that, in the BF1(*trans*-Pro22) case, Ala1−N has an additional hydrogen bond with Pro22. In the evaluation of the possibility of observing this interaction for the *cis*-Pro22 case, we found that it was not detected within the required distance for bonding during the last 250 ps of the trajectory. The loss of this hydrogen bond in the BF1(*cis*-Pro22) appears to provide space for the

Table 2: Displacements (in Å) after Optimal Alignments of the Calcium Ion Positons

| $Ca^{2+}$ | BF1(*trans*-Pro22) vs crystal | BF1(*cis*-Pro22) vs crystal | BF1(*trans*-Pro22) vs BF1(*cis*-Pro22) |
|---|---|---|---|
| 1 | 0.43 | 0.93 | 0.66 |
| 2 | 0.62 | 0.64 | 0.29 |
| 3 | 0.75 | 0.82 | 0.94 |
| 4 | 1.14 | 1.27 | 0.25 |
| 5 | 1.80 | 1.45 | 0.38 |
| 6 | 2.83 | 2.91 | 0.53 |
| 7 | 1.79 | 0.89 | 0.96 |
| RMSD | 1.57 | 1.44 | 0.63 |

slightly closer positioning of the calcium ions around Ala1−N in the case of *cis*-Pro22.

*(B) Calcium*−*Gla Network.* In the presence of calcium, the Gla residues of another vitamin K-dependent (VKD) protein, factor X (6, 7, 16, 20, and 29), fold into the core region which was previously occupied by Phe4, Leu5, and Val8 (*37*). This same folding occurs in BF1 with a Gla−calcium network in which the arrangement of calcium ions is such that the interionic distances among the neighboring ions are between 4 and 6 Å in the crystal structure. The Gla−calcium network and the arrangement of calcium ions were found to be stable for the duration of our simulations. In Table 2, we summarize the displacements of calcium ions with respect to the crystal positions as well as with respect to each other (*trans* versus *cis*), after the optimal alignment of calcium ions. Both *cis* and *trans* systems show relatively similar displacements with respect to the crystal positions, and the displacements are well under an angstrom (on the average) when *trans* and *cis* systems are compared. Out of four calcium ions which have displacements greater than 1 Å in BF1(*trans*-Pro22), two (Ca4 and Ca5) are coordinated with the N-terminal Ala1 residue, and the other two are highly solvent accessible. However, one of the highly solvent accessible calcium ions (Ca7) moved toward the crystal position, in the BF1(*cis*-Pro22).

The calcium ion network is tightly associated with the Gla residues in the Gla domain. The coordination of the calcium ions in this network is summarized in Table 3. Other than solvation, there are no apparent changes found in the calcium coordination and the calcium−Gla network when compared the crystal and solution structures. Interestingly, the network is unchanged in the process of *trans*−*cis* isomerization. Note that Gla20 and Gla21 are adjoining residues to the isomerization site (Pro22).

*(C) Hydrogen Bonding in the Disulfide Loop Region.* Since Pro22 resides in a disulfide loop of six residues, it is natural to examine changes, if any, in the hydrogen bonds associated with these residues in the process of isomerization. This region is also interesting, because it retains hydrogen bonds with the Ala1 residue in the formation of the Ω-loop. Also, as can be seen from the summary in Table 4, this region is in close contact with the hydrophobic stack that connects the Gla region to the thrombin-sensitive region of BF1. Although some of the interactions are not hydrogen bonds in the crystal, all of the corresponding distances in the crystal structure for the donor acceptor pairs found in the solution structures are also shown in this table for comparison. There are six hydrogen bonds found in the loop region of BF1(*trans*-Pro22), but the number reduces to four in BF1(*cis*-Pro22) due to the breakup of Ala1−Pro22 and Gla15−Gla20 hydrogen bonds. However, all forms show strong binding to the N-terminus through Ala1 and to the hydrophobic stack through Tyr45.

*(D) Possible Phospholipid Binding Activity.* Binding of the VKD proteins in the blood coagulation cascade to biological membranes is a pivotal step in the process of coagulation. The activation of most of these proteins takes place on the membrane surface where the binding localizes

Table 3: $Ca^{2+}$−Gla Interactions ($d_{Ca-Gla} \leq 3.0$ Å) for the Crystal (Top Line) and Two Solution Structures of BF1 (*trans*-BF1, Middle Line, and *cis*-BF1, Bottom Line)[a]

| | Gla | | | | | | | | | | | |
|---|---|---|---|---|---|---|---|---|---|---|---|---|
| | Gla7 1234 | Gla8 1234 | Gla15 1234 | Gla17 1234 | Gla20 1234 | Gla21 1234 | Gla26 1234 | Gla27 1234 | Gla30 1234 | water | other | total |
| Ca1 | | | | | | | 0110 | | 1010 | NO[b] | | 4 |
| | | | | | | | 0100 | | 1010 | 4 | | 7 |
| | | | | | | | 0100 | | 1010 | 4 | | 7 |
| Ca2 | | 0101 | | | | | | 0100 | 0011 | 1 | | 6 |
| | | 0101 | | | | | 0100 | 0100 | 0011 | 1 | | 7 |
| | | 0101 | | | | | 0100 | 0100 | 0011 | 1 | | 7 |
| Ca3 | | 0001 | | 1100 | | | | 1000 | 0001 | 2 | | 7 |
| | | 0011 | | 1000 | | | | 1000 | 0001 | 3 | | 8 |
| | | 0011 | | 1000 | | | | 1000 | 0001 | 3 | | 8 |
| Ca4 | 1000 | 0010 | | 1010 | | | | 1001 | | NO | 1 | 7 |
| | 1000 | 0010 | | 1010 | | | | 1001 | | 1 | 1 | 8 |
| | 1000 | 0010 | | 1010 | | | | 1001 | | 1 | 1 | 8 |
| Ca5 | 1100 | | | 0011 | | 0001 | | | | 2 | | 7 |
| | 0100 | | | 0011 | | 0011 | | | | 3 | | 8 |
| | 0100 | | | 0011 | | 0011 | | | | 3 | | 8 |
| Ca6 | | | | | 0100 | 0110 | | | | NO | | 3 |
| | | | | | 1100 | 0100 | | | | 4 | | 7 |
| | | | | | 1100 | 0100 | | | | 4 | | 7 |
| Ca7 | | | 0001 | | 0011 | | | | | NO | | 3 |
| | | | 0011 | | 0011 | | | | | 4 | | 8 |
| | | | 0011 | | 0011 | | | | | 4 | | 8 |

[a] The results were averaged over the last 20 ps of the trajectories. [b] NO = not observed.

Table 4: Comparison of Intramolecular Hydrogen Bonds[a] Associated with the Disulfide Loop Regions of the Solution Structures of *trans*-BF1 and *cis*-BF1[b]

| BF1(*trans*-Pro22) | | | | BF1(*cis*-Pro22) | | | | crystal | | |
|---|---|---|---|---|---|---|---|---|---|---|
| donor | acceptor | *r* (Å) | angle | donor | acceptor | *r* (Å) | angle | donor | acceptor | *r* (Å) |
| Ala1−N | Gla17−OE3 | 2.902 | 141 | Ala1−N | Gla17−OE3 | 2.904 | 136 | Ala1−N | Gla17−OE3 | 2.720 |
| Ala1−N | Gla21−OE4 | 2.893 | 124 | Ala1−N | Gla21−OE4 | 2.886 | 134 | Ala1−N | Gla21−OE4 | 2.910 |
| Ala1−N | Pro22−O | 2.959 | 136 | | | | | Ala1−N | Pro22−OE3 | 3.750 |
| Leu19−N | Leu14−O | 2.981 | 155 | Leu19−N | Leu14−O | 3.019 | 150 | Leu19−N | Leu14−O | 3.020 |
| Gla20−N | Gla15−O | 2.852 | 168 | | | | | Gla20−N | Gla15−O | 2.820 |
| Tyr45−OH | Cys18−O | 2.860 | 150 | Tyr45−OH | Cys22−O | 2.698 | 158 | Tyr45−OH | Cys18−O | 3.980 |

[a] Hydrogen bond criteria used: donor−acceptor distance < 3.10 Å and D−H···A angle > 115°. [b] The results were averaged over the last 20 ps of the trajectories. The corresponding distances in the crystal structure between the donor and acceptor atoms are also shown.

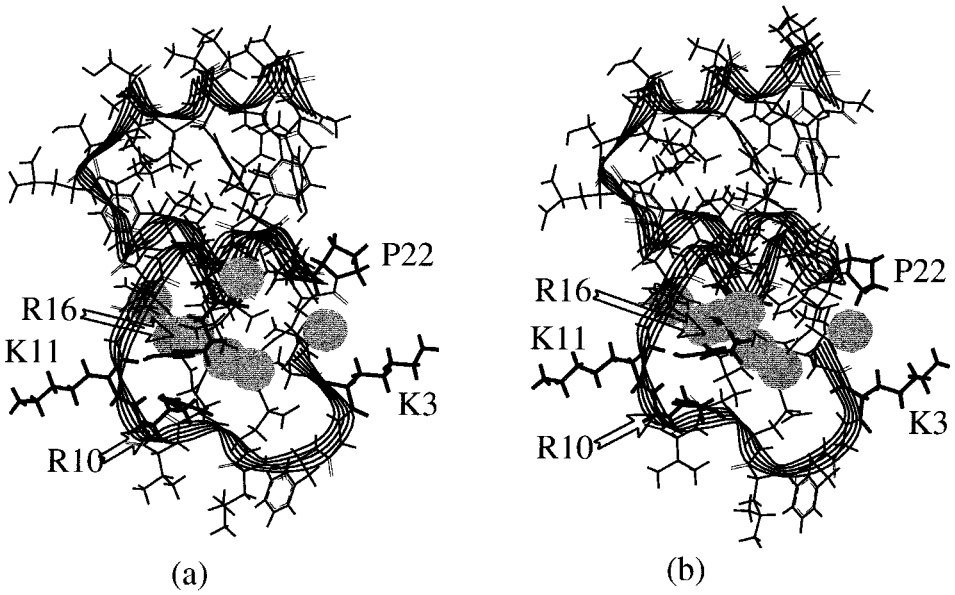


FIGURE 3: Final solution structures of BF1 with (a) *cis*-Pro22 and (b) *trans*-Pro22. As discussed in the text, they represent the general features of the solution structure during the final 20 ps of the trajectories. The backbone ribbons are used to represent the secondary structures of the proteins. Pro22 is marked to highlight its participation in the N-terminal Ala1 network (*trans* conformation). Lys3, Arg10, Lys11, and Arg16 residues are shown specifically to facilitate the discussion on the lipid binding. The calcium ions (4 and 5) that are involved in the N-terminal network are also shown in the figure.

the enzyme−substrate complex. Thus far, experiment and theory identify the major role of calcium ions as inducing the correct fold and in assisting the membrane binding. The Gla domain, which is highly homologous among the VKD proteins in the coagulation cascade, binds calcium ions, and the calcium binding sites of the Gla domain have been well characterized by X-ray crystallographic (*35*, *43*) and solution NMR studies (*12*−*14*) and also by molecular dynamics simulations and homology modeling (*21*−*23*, *31*). However, the manner in which the Gla domain is bound to the membrane surface, and thus the possible participation of Pro22 in the binding process, is still debatable. In one proposal of lipid binding (*29*), simultaneous coordination of the calcium ions to both the negatively charged Gla region of the VKD proteins and the negatively charged phospholipid headgroups (e.g., phosphatidylserine) was advanced. In a supporting scenario, annexin V was experimentally found to be bound to the phosphatidylserine membrane surface with a conformationally specific structure (*38*), in which some calcium ions may have open coordination for lipid binding while bound to the protein. Also, there exists the suggestion that, in addition to the calcium-mediated bridging mechanism, a hydrophobic component to the phospholipid binding of the Gla domain is present. This mechanism depends at least partially on the penetration of some hydrophobic residues into the lipid surface upon calcium binding (*4*, *5*, *8*, *20*, *42*). In a recent model, McDonald et al. (*25*, *26*) proposed a membrane contact mechanism consisting of an isolated protein−lipid ion pair. In the present study, we attempt to elucidate previously debated factors of prothrombin membrane binding using structural comparisons.

We present figures of the final configurations from dynamics simulations for both Pro22 (*cis* and *trans*) systems (analysis of these structures shows that they are representative configurations; see Figure 3). Also, we have evaluated the electrostatic potential energy surfaces for these configurations and present them in Figure 4. Even though Pro22 has direct contact with Ala1 in the *trans* conformation, the structure of the Ω-loop region for both is seen to be well preserved. As has been suggested previously (*1*), the hydrophobic residues (Phe5, Leu6, and Val9) in both cases are aligned in a manner (Figure 3) such that they could directly penetrate into a parallel lipid surface. The same is true of the X-ray crystal structure orientation of these residues.

In an experiment designed to examine the topography of the phospholipid binding sites of BF1, the lysine residues were selectively acetylated in the presence and absence of phospholipids (*2*). Both Lys3 and Lys11 were found to be significantly protected from acetylation in the presence of phospholipids. In both cases, two Lys residues (3 and 11)

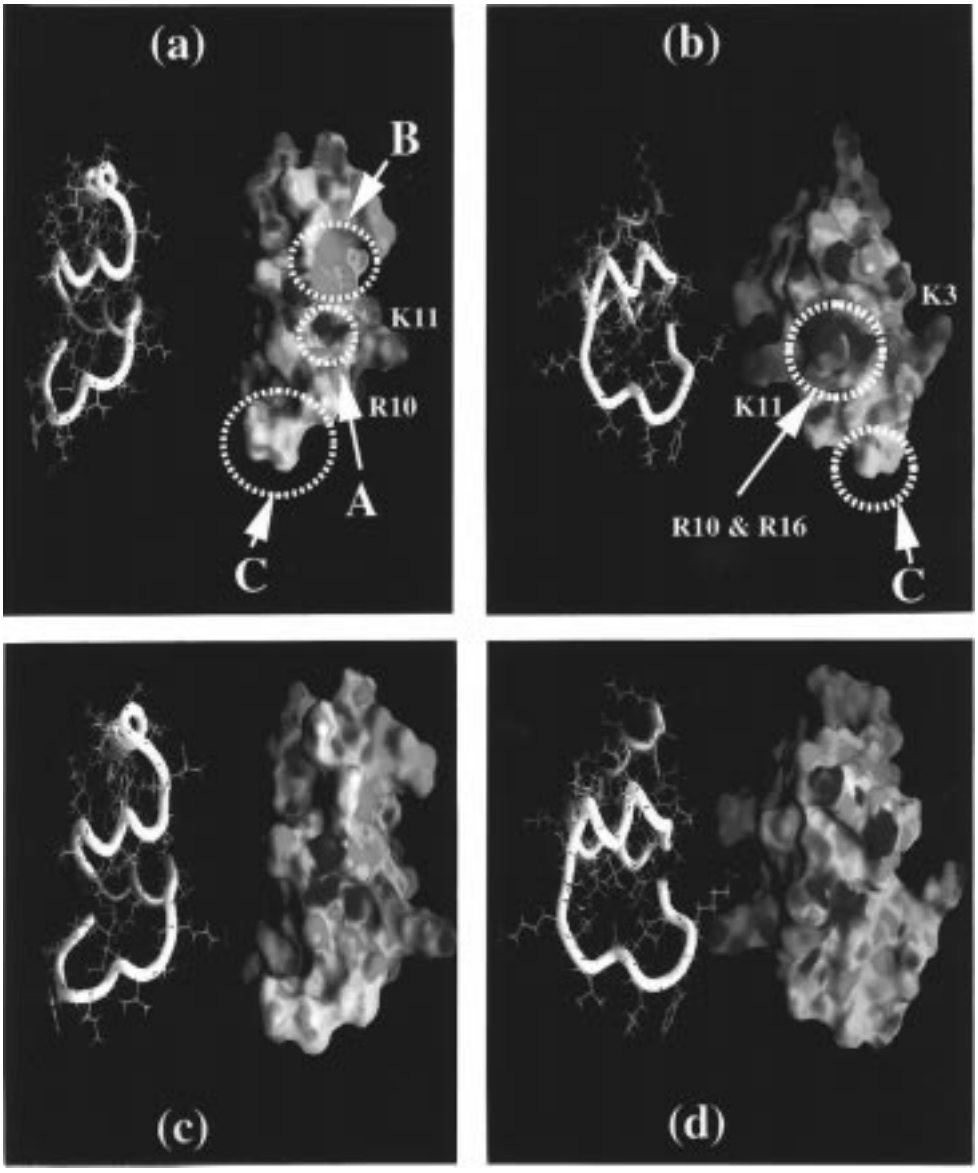


FIGURE 4: Electrostatic potential energy surfaces for BF1 with *trans*-Pro22 and *cis*-Pro22 in their final solution structures (panel b is the back-side view of panel a while panel d is the back-side view of panel c). The energy surfaces are calculated and displayed on the van der Waals surface with the help of the program GRASP (*27*). The charges required for GRASP calculations are directly derived from the AMBER force field. The corresponding solution structures are also displayed in the same orientations as of the potential energy surfaces to trace the important residues in the lipid binding. All the residues of BF1 involved in the computation are used in creating this picture. Also, the total charge of the structure for which the map is constructed is zero. Panels a and b correspond to the *trans* structure while panels c and d correspond to the *cis* structure. Interesting regions and important residues are marked only on panels a and b for clarity in the comparison. Regions A, B, and C correspond to the pore described by McDonald et al. (*26*), the position of the eighth calcium determined by Seshadri et al. (*34*), and the hydrophobic residues in the Ω-loop, respectively.

are solvent exposed (Figure 3) and predicted to potentially participate in the direct interaction with the zwitterionic lipid headgroups. Note that BF1 is the only protein in the coagulation cascade other than factor IX to have a charged residue prior to the first Gla residue in the N-terminal region.

Arg16 is found in all the VKD proteins except protein Z for which Arg is replaced by another basic residue, Lys. Zhang et al. (*41*) demonstrated the importance of this residue in lipid binding through the mutation of this residue in protein C to Leu, with the resulting loss of lipid binding. Likewise, Thariath and Castellino (*39*) suggested this as a critical residue in the Gla domain of protein C (and perhaps in other VKD proteins since it is conserved) for the adoption of a calcium-dependent conformation that allows lipid binding. They used a model of the Gla domain of protein C based on the X-ray crystal structure of BF1 (*35*) to emphasize the importance of the H-bonding between Arg15 and both Gla16 and His10 for maintaining the conformational integrity of the calcium−Gla complex. In the present study, the corresponding Arg residue in both conformations (*cis*- and *trans*-Pro22) is found to maintain H-bonding with Gla17 and Lys11 during the period of simulations. However, Arg16 is somewhat solvent exposed for both *cis*/*trans*-Pro22 regardless of its involvement in the H-bonding with the neighboring residues. Arg10 is in the vicinity of Arg16 and is highly solvent accessible. This residue lies normal to the plane of the Ω-loop and somewhat parallel to Arg16. The environment of these residues may provide an opportunity to participate in the direct lipid binding through salt bridges,

but whatever the interaction, it should be the same for both *cis*/*trans*-Pro22.

One interesting development is the recently proposed model (see below) in which an ion pair mechanism is invoked in binding (*25*, *26*). We use the electrostatic potential surfaces using the program GRASP (*27*) (Figure 4) to compare *cis* and *trans* electrostatics in the context of the McDonald model. We have mapped the electrostatic potential surface to the van der Waals surface of the atomic entities, and for each configuration (*cis* and *trans*), we display both the front (panels a and c) and back (panels b and d) views for clarity. Both potential surfaces (*cis* and *trans*) appear similar, and considering that there is no significant difference in the secondary structure for the two forms, this is not surprising. The blue cavity marked by circle A is the pore (attractive to phospholipids) described by McDonald et al. (*25*, *26*). This pore is also well preserved in both *cis* and *trans* conformations. Some surface-exposed calcium ions are also seen around the pore as blue patches. Above this region there exists a prominent electronegative region (a large red region marked by circle B) where the eighth strontium ion found in the work of Tulinsky group is located (*34*). Prominent electropositive patches (shown in blue) are mainly around residues Lys3 and Lys11 (finger-like surfaces in panels b and d) and Arg10 and Arg16 (marked in the panel b) marking a blue band across the protein surface. This band is found to be in the back side of the pore described above. These areas may also be potential candidate regions for negatively charged lipid to be bound. On the other hand, the region which contains the hydrophobic residues (Phe5, Leu6, and Val9) is found to be electrostatically neutral, supporting the possibility of the insertion of these residues into the lipid surface. This finding that the hydrophobic residues in the Ω-loop (regions marked by circle C) are electrically neutral is somewhat at odds with a recent work (*26*) in which this region is argued to be substantially electronegative. It will be interesting to apply yet to be developed theoretical or experimental methods to resolve this question.

## CONCLUSIONS

We have used molecular dynamics simulations to estimate solution structure details on the isomerization of Pro22 in BF1 from the *trans* to *cis* conformation. The secondary structure, the calcium−Gla network, the Ala1 network, and the H-bond network of the disulfide loop comprised of residues 17−23 remain largely unaltered during the isomerization reaction. Also, energies associated with the two systems are comparable. Thus, our earlier estimate of $\Delta G°$ (*trans* → *cis*) of −17 kcal/mol, found using cutoffs on the electrostatic interactions, is not substantiated with the improved methodology and higher resolution in the starting structure. On the basis of these observations, we conclude that if isomerization of Pro22 is required for phospholipid binding, the isomerization may take place without a structural penalty. However, we know that the X-ray crystal structure has Pro22 in the *trans* conformation (at high $Ca^{2+}$ concentration), we know that a long simulation (800 ps) started in this form does not revert to *cis*, we know that Pro occurs at position 22 only in BF1 (other VKD proteins bind phospholipid in the presence of $Ca^{2+}$), and we find no significant structural difference between *cis* and *trans* forms that would imply a functional difference. Thus, although it appears that the calculated free energy difference between *cis* and *trans* forms would permit the *cis* form to occur if the activation barrier could be overcome, there is little apparent evidence to suggest that this happens. Whether the presence of phospholipid tilts the *cis*−*trans* equilibrium remains to be resolved.

## ACKNOWLEDGMENT

We have benefited from the valuable discussions with Professor Gary L. Nelsestuen at the University of Minnesota, who suggested this study. A reviewer provided key questions that were most helpful. We acknowledge the computational resources provided by the North Carolina Supercomputing Center, the National Cancer Institute, the Pittsburgh Supercomputing Center, and the NIH-sponsored Computational Structural Biology Resource, Biochemistry, UNC, Chapel Hill. We thank Dr. Lars Nyland for helping with software implementations on the NIH Biological Resource Facility at UNC, Chapel Hill.

## REFERENCES

1. Arni, R. K., Padmanabhan, K., Padmanabhan, K., P., Wu, T. P., and Tulinsky, A. (1994) *Chem. Phys. Lipids 67*, 59−66.
2. Birdwell, K. R. (1994) Ph.D. Dissertation, University of North Carolina, Chapel Hill.
3. Charifson, P. S., Darden, T., Tulinsky, A., Hughey, J. L., Hiskey, R. G., and Pedersen, L. G. (1991) *Proc. Natl. Acad. Sci. U.S.A. 88*, 424−428.
4. Christiansen, W. T., Tulinsky, A., and Castellino, F. J. (1994) *Biochemistry 33*, 14993−15000.
5. Christiansen, W. T., Jalbert, L. R., Robertson, R. M., Jhingan, A., Prorok, M., and Castellino, F. J. (1995) *Biochemistry 34*, 10376−10382.
6. Cornell, W. D., Cieplak, P., Bayly, C. I., Gould, I. R., Merz, K. M., Jr., Ferguson, D. M., Spellmeyer, D. C., Fox, T., Caldwell, J. W., and Kollman, P. A. (1995) *J. Am. Chem. Soc. 117*, 5179−5197.
7. Deber, C. M. Fossel, E. T., and Blout, E. R. (1974) *J. Am. Chem. Soc. 96*, 4015−4017.
8. Ellison, E. H., and Castellino, F. J. (1997) *Biophys. J. 72*, 2605−2615.
9. Essmann, U., Perera, L., Berkowitz, M. L., Darden, T., Lee, H., and Pedersen, L. G. (1995) *J. Chem. Phys. 103*, 8577−8593.
10. Evans, T. C., Jr., and Nelsestuen, G. L. (1996) *Biochemistry 35*, 8210−8215.
11. Francart, C., Eieruszeski, J.-M., Tarter, A., and Lippens, S. (1996) *J. Am. Chem. Soc. 118*, 7019−7027.
12. Freedman, S. J., Furie, B. C., Furie, B., and Baleja, J. D. (1995) *Biochemistry 34*, 12126−12137.
13. Freedman, S. J., Furie, B. C., Furie, B., and Baleja, J. D. (1995) *J. Biol. Chem. 270*, 7980−7987.
14. Freedman, S. J., Blostein, M. D., Baleja, J. D., Jacobs, M., Furie, B. C., and Furie, B. (1996) *J. Biol. Chem. 271*, 16227−16236.
15. Hamaguchi, N., Cherifson, P., Darden, T., Xiao, L., Padmanabhan, K., Tulinsky, A., Hiskey, R., and Pedersen, L. (1992) *Biochemistry 31*, 8840−8848.
16. Hodel, A., Rice, L. M., Simonson, T., Fox, R. O., and Brunger, A. T. (1995) *Protein Sci. 4*, 636−654.
17. Ikura, T., Tsurupa, G. P., and Kuwajima, K. (1997) *Biochemistry 36*, 6529−6538.
18. Kay, J. E. (1996) *Biochem. J. 314*, 361−385.
19. Lavitt, M. (1981) *J. Mol. Biol. 145*, 251−263.
20. Lecompte, M. F., and Dode, C. (1992) *Bioelectrochem. Bioenerg. 29*, 149−157.
21. Li, L., Darden, T., Foley, C., Hiskey, R., and Pedersen, L. (1995) *Protein Sci. 4*, 2341−2348.

22. Li, L., Darden, T., Hiskey, R., and Pedersen, L. (1996) *J. Chem. Phys. 100*, 2475−2479.
23. Li, L., Darden, T. A., Freedman, S. J., Furie, B. C., Furie, B., Baleja, J. D., Smith, H., Hiskey, R. G., and Pedersen, L. G. (1997) *Biochemistry 36*, 2132−2138.
24. Marsh, H. C., Scott, M. E., Hiskey, R. G., and Koehler, K. A. (1979) *Biochem. J. 183*, 513−517.
25. McDonald, J. F., Shah, A. M., Schwalbe, R. A., Kisiel, W., Dahlback, B., and Nelsestuen, G. L. (1997) *Biochemistry 36*, 5120−5127.
26. McDonald, J. F., Evans, T. C., Jr., Emeagwali, D. B., Hariharan, M., Allewell, N. M., Pusey, M. L., Shah, A. M., and Nelsestuen, G. L. (1997) *Biochemistry 36*, 15589−15598.
27. Nicholls, A., Sharp, K., and Honig, B. (1991) *Proteins 11*, 281−296.
28. Nelsestuen, G. L. (1976) *J. Biol. Chem. 251*, 5648−5656.
29. Nelsestuen, G. L. (1988) in *Current Advances in Vitamin K Research* (Suttie, J. W., Ed.) pp 335−339, Elsevier Scientific Publishing Co., Inc., New York.
30. Pearlman, D. A., Case, D. A., Caldwell, J. W., Ross, W. S., Cheatham, T. E., III, Ferguson, D. M., Seibel, G. L., Singh, U. C., Weiner, P. K., and Kollman, P. A. (1995) *AMBER 4.1*, University of California, San Francisco.
31. Perera, L., Li, L., Darden, T., Monroe, D. M., and Pedersen, L. G. (1997) *Biophys. J. 73*, 1847−1856.
32. Pollock, J. S., Shepard, A. J., Weber, D. J., Olson, D. L., Klapper, D. G., Pedersen, L. G., and Hiskey, R. G. (1988) *J. Biol. Chem. 263*, 14216−14223.
33. Schreiber, G., and Fersht, A. (1993) *Biochemistry 32*, 11195−11203.
34. Seshadri, T., Skrzypczak-Jankun, E., Yin, M., and Tulinsky, A. (1994) *Biochemistry 33*, 1087−1092.
35. Soriano-Garcia, M., Padmanabhan, K., de Vos, A. M., and Tulinsky, A. (1992) *Biochemistry 31*, 2554−2566.
36. Soriano-Garcia, M., Park, C. H., Tulinsky, A., Ravichandran, K. G., and Skrzypczak-Jankun, E. (1989) *Biochemistry 28*, 6805−6810.
37. Sunnerhagen, M., Forsen, S., Hoffren, A.-M., Drakenberg, T., Teleman, O., and Stenflo, J. (1995) *Nat. Struct. Biol. 2*, 504−509.
38. Swairjo, M. A., Concha, M. A., Kaetzel, J. R., Dedman, J. R., and Seaton, B. A. (1995) *Nat. Struct. Biol. 2*, 968−974.
39. Thariath, A., and Castellino, F. J. (1997) *Biochem. J. 322*, 309−315.
40. Welsch, D. J., and Nelsestuen, G. L. (1988) *Biochemistry 27*, 4939−4945.
41. Zhang, L., Jhingan, A., and Castellino, F. J. (1992) *Blood 80*, 942−952.
42. Zhang, L., and Castellino, F. J. (1994) *J. Biol. Chem. 269*, 3590−3595.
43. Banner, D. W., D'Arcy, A., Chene, C., Winkley, F. K., Guha, A., Konigsberg, W. H., Nemerson, Y., and Kirchhofer, D. (1996) *Nature 380*, 41−46.

BI980263U